INTERNATIONAL JOURNAL FOR NUMERICAL METHODS IN FLUIDS
Int. J. Numer. Meth. Fluids **28**: 1053–1071 (1998)

COMPUTATION OF INTERNAL HIGH-SPEED SEPARATED FLOW WITH MODIFIED B–L AND J–K MODELS

Y. ZHAO* AND Z.M. DING

School of Mechanical and Production Engineering, Nanyang Technological University, Nanyang Avenue, Singapore 639798, Singapore

SUMMARY

The existence of shock–turbulent boundary layer interactions lead to very complicated flow phenomena and pose a challenge for numerical simulation. In this paper, two turbulence models, the Baldwin–Lomax (B–L) model and the Johnson–King (J–K) model, which were originally developed for simple external flow simulation, are modified to model complex high-speed internal separated flows. The full Navier–Stokes solver used in this paper is based on a cell-centered finite volume method and multistepping time marching scheme. Both implicit residual smoothing and local time stepping techniques are incorporated to accelerate the convergence rate. To ensure the numerical stability with the present explicit scheme, a point-implicit treatment to the source term in the ordinary differential equation (ODE) of the J–K model has been developed and has proved to be very effective in modeling such a complex flow. An arc-bump channel flow case has been studied. Comparisons of computed results with experimental data show that the present solver, with the modified turbulence models, predicts the shock and the flow separation very well. The J–K model is found to predict the size of the separation bubble with a higher accuracy. © 1998 John Wiley & Sons, Ltd.

KEY WORDS: turbulence modeling; internal flow; flow separation; shock–boundary layer interaction; finite volume method

1. INTRODUCTION

High-speed turbulent flows in ducts can be found in various engineering applications, such as the propulsion system of aircraft. The main difficulties in numerically simulating such flows stem from the complexity of the flow physics. Both the complicated geometry of the flow domain and the compressibility of the flow, can lead to flow features such as shock, shock–boundary layer interactions and subsequent flow separation. The interaction between shock and boundary layer often occurs in transonic turbulent flow cases. For the simulation of these flows, turbulence modeling has a crucial influence on the predictive capability of any solver. In the present research, a quasi-three-dimensional (Q3D) arc-bump channel flow is investigated by using the modified Baldwin–Lomax (B–L) and Johnson–King (J–K) models.

The Baldwin–Lomax model [1] was proposed in 1983 and has been mostly applied in external turbulent flows, both incompressible and compressible. Its advantages are its simplic-

* Correspondence to: School of Mechanical and Production Engineering, Nanyang Technological University, Nanyang Avenue, Singapore 639798, Singapore.

CCC 0271–2091/98/171053–19$17.50

Received August 1996
Revised April 1997

ity and, in some sense, generality. In many practical engineering computations, this model has played an important role. For some complicated flows, however, it is also necessary to introduce some modifications to this model in order to obtain satisfactory results. It is well-known that the B–L model is an equilibrium turbulence model due to the assumption of a balance between the production and dissipation of turbulence. But for most flows, this assumption is not valid and the diffusion and convection of turbulence must be taken into account. On the other hand, if the flow has separation, the B–L model will lead to an incorrect evaluation of the turbulent viscosity. Several modifications have been proposed to overcome these deficiencies of the model. Some of them are adopted in this paper to improve the capability and efficiency of the present solver.

Drawbacks of the B–L model are obvious, as mentioned above. To consider the influence of the diffusion and convection of turbulence, a new algebraic model was proposed, based on the B–L model, by Johnson and King [2] in 1985. In this model, an ordinary differential equation (ODE) is used to describe the history effect of turbulence. Therefore, the J–K model is theoretically closer to the flow physics than the B–L model. When the J–K model was applied to some separated flow computations, the results were much better than those by the B–L model. Since both models were originally proposed to tackle external turbulent flow problems, certain modifications are necessary for their applications to internal flows.

Bump channel flows have been widely used as benchmarks for validating various solvers; this class of flow has complicated physical phenomena such as shock and flow separation, induced by the streamline curvature and/or the shock–boundary layer interaction [3,4]. All of these features are severe challenges to turbulence modeling, as well as the numerical strategy. In the present study, an arc-bump channel flow [5] is investigated by an explicit solver with two kinds of turbulence models: the B–L model and the J–K model. The problems encountered in the present computation are due to the flow complexity and the existence of multiple walls. In this study, the main drawbacks of both models are discussed and some solutions proposed by other researchers are incorporated. A separated-wall integration strategy is presented here to deal with multiple walls in the channel flow computation using the J–K model. A point-implicit treatment to the source term of the ODE in the J–K model is proposed and shown to be necessary to obtain stable and convergent solutions. The computed result shows a satisfactory agreement with the experimental data.

2. THE MATHEMATICAL DESCRIPTION AND NUMERICAL ALGORITHMS

2.1. Governing equations

The Reynolds-averaged Navier–Stokes (RANS) in a Cartesian co-ordinate system can be written as

$$\frac{\partial W}{\partial t}+\frac{\partial F_c}{\partial x}+\frac{\partial G_c}{\partial y}+\frac{\partial H_c}{\partial z}=\frac{\partial F_v}{\partial x}+\frac{\partial G_v}{\partial y}+\frac{\partial H_v}{\partial z}, \tag{1}$$

where W is the vector of dependent variables, F_c, G_c and H_c are the convective flux vectors, and F_v, G_v and H_v are the viscous flux vectors. They are given by

$$W=\begin{bmatrix}\rho\\ \rho u\\ \rho v\\ \rho w\\ \rho E\end{bmatrix},\qquad \vec{F}_{\mathrm{c}}=\begin{bmatrix}\rho\vec{U}\\ \rho u\vec{U}+p\vec{i}\\ \rho v\vec{U}+p\vec{j}\\ \rho w\vec{U}+p\vec{k}\\ \rho H\vec{U}\end{bmatrix},\qquad \vec{F}_{\mathrm{v}}=\begin{bmatrix}0\\ \vec{\tau}_x\\ \vec{\tau}_y\\ \vec{\tau}_z\\ \bar{\bar{\tau}}\cdot\vec{U}-\vec{q}\end{bmatrix}, \tag{2}$$

where the following definitions are used:

$$\vec{F}_{\mathrm{c}}=F_{\mathrm{c}}\vec{i}+G_{\mathrm{c}}\vec{j}+H_{\mathrm{c}}\vec{k},$$

$$\vec{F}_{\mathrm{v}}=F_{\mathrm{v}}\vec{i}+G_{\mathrm{v}}\vec{j}+H_{\mathrm{v}}\vec{k},$$

$$\rho E=\rho e+\frac{1}{2}\rho(u^2+v^2+w^2),$$

$$\bar{\bar{\tau}}=\vec{\tau}_x\vec{i}+\vec{\tau}_y\vec{j}+\tau_z\vec{k},$$

$$\vec{\tau}_i=\tau_{ix}\vec{i}+\tau_{iy}\vec{j}+\tau_{iz}\vec{k},$$

$$\vec{q}=-c_p\left(\frac{\mu_l}{Pr_l}+\frac{\mu_t}{Pr_t}\right)\vec{\nabla}T.$$

In integral form, Equation (1) can be rewritten as

$$\frac{\partial}{\partial t}\int_\Omega W\,\mathrm{d}V+\int_{\partial\Omega}\vec{F}_{\mathrm{c}}\cdot\vec{n}_{\mathrm{s}}\,\mathrm{d}S=\int_{\partial\Omega}\vec{F}_{\mathrm{v}}\cdot\vec{n}_{\mathrm{s}}\,\mathrm{d}S. \tag{3}$$

The above system of equations is closed by the state equation of a perfect gas, i.e.

$$p=\rho(\gamma-1)e. \tag{4}$$

All the governing equations are written in non-dimensional form by using a reference length and free stream flow conditions.

2.2. Discretization

The cell-centered finite volume technique is employed to discretize the special operators in the governing equations in integral form. This reduces the governing equations to a set of ODEs, which are in turn, solved by an explicit multistage Runge–Kutta time marching scheme proposed by Jameson *et al.* [6]. The three-dimensional flow domain is divided into a large number of hexahedral subdomains or cells. The integral form accepts the existence of flow discontinuities in the flow field, and the finite volume approach ensures the conservation of mass, momentum and energy over all these small finite volumes, while the average rate of change of W in each are calculated. After the finite volume discretization based on the center-difference scheme, the integral Navier–Stokes equation (3) becomes

$$\begin{aligned}\frac{\mathrm{d}}{\mathrm{d}t}(W)_k&=-\frac{1}{\Delta V_k}\left(\sum_{f=1}^{6}(\vec{F}_{\mathrm{c}}\cdot\vec{n}\Delta S)_f-\sum_{f=1}^{6}(\vec{F}_{\mathrm{v}}\cdot\vec{n}\Delta S)_f\right)=-\frac{1}{\Delta V_k}[Q_{\mathrm{c}}(W)-Q_{\mathrm{v}}(W)]\\&=-R(W)_k.\end{aligned} \tag{5}$$

Here the net convective and viscous fluxes are

$$Q_{\mathrm{c}}(W)=\sum_{f=1}^{6}(\vec{F}_{\mathrm{c}}\cdot\vec{n}\Delta S)_f,\qquad Q_{\mathrm{v}}(W)=\sum_{f=1}^{6}(\vec{F}_{\mathrm{v}}\cdot\vec{n}\Delta S)_f. \tag{6}$$

In the above equations, ΔV_k is the volume of a cell k and $\Delta\vec{S} = \vec{n}\Delta S$ is the area vector of one of its six cell faces, with f denoting the fth one and its direction being outward normal to f. $\vec{n}$ is the outward normal vector on the face S. $R(W)$ is the vector of residuals. Fluxes at cell surfaces are evaluated by the center-difference scheme.

The viscous fluxes required on the cell interfaces contain first derivatives of flow variables, which are calculated using a local co-ordinate transformation from Cartesian co-ordinates (x, y, z) to the curvilinear co-ordinates (ξ, η, ζ) in the three grid line directions. For a scalar ϕ, its derivative with respect to x_i $(i = 1, 2, 3)$ on face f is calculated as

$$(\phi_{x_i})_f = \left(\frac{\partial\phi}{\partial\xi}\frac{\partial\xi}{\partial x_i} + \frac{\partial\phi}{\partial\eta}\frac{\partial\eta}{\partial x_i} + \frac{\partial\phi}{\partial\zeta}\frac{\partial\zeta}{\partial x_i}\right)_f.$$

The derivatives ϕ_ξ, ϕ_η and ϕ_ζ are approximated using finite differences. For example,

$$\left.\frac{\partial\phi}{\partial\xi}\right|_{I+1/2,J,K} = \phi_{I+1,J,K} - \phi_{I,J,K},$$

$$\left.\frac{\partial\phi}{\partial\eta}\right|_{I+1/2,J,K} = \phi_{I+1/2,J+1/2,K} - \phi_{I+1/2,J-1/2,K},$$

$$\left.\frac{\partial\phi}{\partial\zeta}\right|_{I+1/2,J,K} = \phi_{I+1/2,J,K+1/2} - \phi_{I+1/2,J,K-1/2}.$$

Here quantities located at corners are calculated by averaging those of the surrounding four cells. The metric coefficients $\xi^i_{x_i}$ found in the above equations can be calculated as

$$(\vec{\nabla}\xi)_f = \left(\frac{\vec{r}_\eta \times \vec{r}_\zeta}{J^{-1}}\right)_f,$$

$$(\vec{\nabla}\eta)_f = \left(\frac{\vec{r}_\zeta \times \vec{r}_\xi}{J^{-1}}\right)_f,$$

$$(\vec{\nabla}\zeta)_f = \left(\frac{\vec{r}_\xi \times \vec{r}_\eta}{J^{-1}}\right)_f,$$

$$(J^{-1})_f = (\vec{r}_\zeta \times \vec{r}_\xi \cdot \vec{r}_\eta)_f.$$

It should be noted that (I, J, K) denotes the centre of the cell (I, J, K), while (i, j, k) represents a grid node at the lower-left corner on the south face of cell (I, J, K). The three covariant-based vectors are computed on the face f in order to calculate the above metric coefficients; for instance, the three vectors on face f, in order to calculate the above metric coefficients.

2.3. Artificial viscosity

In order to avoid odd–even point decoupling and oscillations near shockwaves, artificial viscosity is needed in the numerical solutions of RANS equations, although theoretically it is unnecessary. Artificial dissipation terms used in this report are based on the work of Jameson *et al.* [6]. An adaptive blending of the second and fourth differences are used to construct the artificial viscosity that provides third-order background dissipation in smooth regions and first-order dissipation at shocks. The dissipation terms can be written as

$$D_{I+1/2}(W) = \max\left(\frac{M}{M_\infty}, 1\right)\bar{\lambda}^\xi_{I+1/2}[\epsilon^{(2)}_{I+1/2}\delta W_{I+1/2} - \epsilon^{(4)}_{I+1/2}(\delta^2 W_{I+1} - \delta^2 W_I)], \tag{7}$$

where δ and δ^2 are the first- and second-center-difference operators. $\bar{\lambda}^{\xi}$ is a scaling factor based on the spectral radii of flux Jacobian matrix in the ξ-direction. The pressure is used as a sensor for shocks and so the coefficients $\epsilon^{(2)}$ and $\epsilon^{(4)}$ are determined by

$$\epsilon^{(2)}_{I+1/2} = \kappa^{(2)} \max(v_{I-1}, v_I, v_{I+1}, v_{I+2}), \tag{8}$$

$$\epsilon^{(4)}_{I+1/2} = \max(0, \kappa^{(4)} - \epsilon^{(2)}_{I+1/2}), \tag{9}$$

where $\kappa^{(2)}$ and $\kappa^{(4)}$ are constants.

The value ranges of $1/2 < \kappa^{(2)} < 1$ and $1/512 < \kappa^{(4)} < 1/64$ are commonly used in calculations. The shock sensor is defined as

$$v_I = \left| \frac{p_{I+1} - 2p_I + p_{I-1}}{p_{I+1} + 2p_I + p_{I-1}} \right|. \tag{10}$$

The dissipation terms in the η- and ζ-directions are defined in a similar way. It should be noted that (I, J, K) denotes the center of a cell.

2.4. Time stepping scheme

The spatially discretized Equation (5) is a system of ODEs in time that are integrated with a five-stage Runge–Kutta scheme. A general m-stage scheme to advance solutions from the nth time step to the $(n+1)$th step, given as n from the nth time step to the next step, can be written as

$$\begin{aligned}
W^{(0)} &= W^n, \\
W^{(1)} &= W^{(0)} - \alpha_1 \Delta t R^{(0)}(W), \\
&\vdots \\
W^{(m-1)} &= W^{(0)} - \alpha_{m-1} \Delta t R^{(m-2)}(W), \\
W^{(m)} &= W^{(0)} - \alpha_m \Delta t R^{(m-1)}(W), \\
W^{(n+1)} &= W^{(m)},
\end{aligned}$$

where

$$R^{(1)} = [(Q_c(W^{(0)}) - Q_v(W^{(0)}))/\Delta V_k - D(W^{(0)})],$$

and

$$R^{(q)} = [(Q_c(W^{(q-1)}) - Q_v(W^{(q-1)}))/\Delta V_k - D(W^{(1)})], \quad q > 1.$$

For a five-stage scheme, the stage coefficients are

$$\alpha_1 = 1/4, \qquad \alpha_2 = 1/6, \qquad \alpha_3 = 3/8, \qquad \alpha_4 = 1/2, \qquad \alpha_5 = 1.$$

In the present code, several approaches have been adopted for the calculation of viscous terms and artificial viscosity terms. One is that the viscous fluxes are updated at every time step, while artificial viscosity is only calculated at the first stage and then frozen for the rest of the stages. For different flow, the careful use of these approaches would result in the fastest convergence.

2.5. Acceleration techniques

2.5.1. Local time stepping. Local time stepping is used to accelerate the convergence to steady state solutions. This means that as large a time step as possible, at each cell, is used, unless the calculation fails to be convergent to the true physical solution. The length of the local time step at a cell is determined by the local values of the dependent variables.

2.5.2. Implicit residual smoothing. The basic idea of implicit residual smoothing is to use an implicit averaging calculation of residuals for increasing the maximum CFL number. Normally, the CFL number can be increased by a factor of 2 or 3. The implicit smoothing equation can be expressed as a factorized form,

$$(1-\epsilon_i\delta_i^2)(1-\epsilon_j\delta_j^2)(1-\epsilon_k\delta_k^2)\bar{R}(W)=R(W), \tag{11}$$

where $\bar{R}(W)$ is the smoothed residual, R is the original residual coefficient for the three grid line directions. ϵ_i, ϵ_j and ϵ_k are the smoothing coefficients for the three grid line directions. In some viscous flows, high aspect ratio cells have to be used to resolve the boundary layer or viscous sublayer. In this situation, the constant smoothing coefficients in Equation (11) should be replaced by the variable ones based on the spectral radii in the three directions.

In the present study, the implicit residual smoothing is applied to the first, third and fifth stages only. Numerical tests have proved that this treatment has no effect on the robustness of the scheme.

3. TURBULENCE MODELS

3.1. The B–L model

3.1.1. Formulations. The B–L algebraic turbulence model [1] is one of the simplest eddy viscosity models, where the turbulent viscosity is algebraically modeled in terms of flow geometry and mean flow variables, and the influence on the mean flow equation by the turbulent kinetic energy is neglected. It is a two layer model, where the turbulent viscosity in the inner layer is determined by using the Prandtl mixing length, and the viscosity in the outer layer is determined from the mean flow and a length scale. The strain rate parameter in the Prandtl mixing length model is replaced by the magnitude of the vorticity.

In the B–L model, the turbulent viscosity is given by

$$\mu_t=\begin{cases}(u_t)_i, & n\le n_c\\ (\mu_t)_0, & n\ge n_c\end{cases}, \tag{12}$$

where n is the normal distance to the wall and n_c is the smallest value of n at which the inner and outer viscosities are equal. In the inner region of the boundary layer, the viscosity is

$$(\mu_t)_i=\rho l^2|\vec{\omega}|, \tag{13}$$

where

$$l=kn(1-e^{-n^+/A^+}), \tag{14}$$

$$n^+=\frac{\sqrt{\rho_w\tau_w}}{\mu_w}n, \tag{15}$$

and

$$\vec{\omega} = \nabla \times \vec{U}. \tag{16}$$

In the outer region,

$$(\mu_t)_o = KC_{cp}\rho F_{wake} F_{Kleb}(n), \tag{17}$$

where F_{wake} is the smaller of

$$\begin{cases} n_{max} F_{max} \\ C_{wk} n_{max}(u^2 + v^2 + w^2)/F_{max} \end{cases}. \tag{18}$$

The term n_{max} is the value of n corresponding to the maximum value of F, F_{max} across the layer, where

$$F(n) = n|\omega|(1 - e^{-n^+/A^+}) \tag{19}$$

and

$$F_{Kleb} = \left[1 + 5.5\left(\frac{nC_{Kleb}}{n_{max}}\right)^6\right]^{-1}. \tag{20}$$

The constants used here are $A^+ = 26$, $C_{wk} = 0.25$, $C_{cp} = 1.6$, $k = 0.41$, $C_{Kleb} = 0.3$, $K = 0.0168$.

3.1.2. Drawbacks and modifications of the B–L model. Some problems with the B–L turbulence model are encountered when it is applied to the computation of internal flows, especially high-speed turbulent flows that may have flow separations, shockwaves and even secondary flow. Here, these drawbacks are highlighted and modifications to it are introduced.

(1) In the flow separation region, it is difficult to determine the maximum value of $F(n)$ because more than one local maximum value can be found across the boundary layer. If a global maximum value is used, the computed turbulence viscosity might be wrong, because the one needed in this model is the first maximum value of $F(n)$ near the wall. This problem was first analyzed by Degani and Schiff [7]. They found that the behavior of $F(n)$ is different for the attached flow region and the separated flow region. They proposed a modification to the original B–L model. A peak value is decided when the value of $F(n)$ drops to 90% of the local maximum value.

(2) In the original B–L model, u_τ was defined as the wall shear velocity, $\sqrt{\tau_w/\rho_w}$. This definition will introduce an incorrect evaluation of turbulence viscosity at the wall when there is flow separation. In fact, $u_\tau = \sqrt{\tau_w/\rho_w}$ is zero at a separation point. This will result in $\mu_t = 0$ in this region. Following the suggestion proposed by Marx [8], a different definition of u_τ is used here, $u_\tau = \max\sqrt{(\mu|\omega|/\rho)}$. This ensures u_τ is greater than zero.

Another solution for this problem, given by Radespiel [9], is to define u_τ by using the maximum value of the laminar shear stress across the boundary layer, as $u_\tau = \sqrt{\tau_{l,max}/\rho_w}$. This is also aimed at ensuring a non-zero value of turbulent viscosity at a separation point.

(3) Since the B–L model is an equilibrium model, it is not suited for separated flows. In the separation region, the production and dissipation of turbulence are not in equilibrium, so the diffusion and convection of turbulence should be taken into account. It is suggested that some non-equilibrium models ought to be applied to obtain more accurate results. Goldberg and Chakravarthy [10] proposed an algebraic k–ϵ turbulence model in which the inner layer viscosity is evaluated by a new formula instead of the Baldwin–Lomax one. In this study, both Degani and Schiff's [7] and Marx's [8] modifications have been employed.

3.2. The J–K model

3.2.1. Formulations. Algebraic turbulence models perform unsatisfactorily in the calculation of separated flows because of the assumption that the local turbulent production and dissipation rates are in equilibrium. For better flow predictions, non-equilibrium effects must be considered to properly describe the actual physical phenomenon. The J–K model is a non-equilibrium turbulence model, first proposed by Johnson and King [2] for two-dimensional external flows. Since this model takes the history effects of the turbulence into account with an ODE for the maximum of Reynolds shear stress, it has been found to perform well for transonic flows with strong viscous inviscid interactions [11]. Abid *et al.* [12] extended the J–K model to three-dimensional thin shear layer flows, and used it to calculate separated transonic wing flows. Their results showed that the non-equilibrium form does play an important role in accurately predicting the transonic separated flows.

In the J–K formulation, the inner layer viscosity is calculated by using a completely different way while the outer layer viscosity computation still remains the same as that used in B–L model, except for a multiplying factor σ. In the outer layer, the viscosity is given by

$$(\mu_t)_o = \sigma\rho K C_{cp} F_{wake} F_{Kleb}(n). \tag{21}$$

The inner layer viscosity can be calculated as

$$(\mu_t)_i = \rho D^2 \kappa n \tau_m^{1/2}. \tag{22}$$

Then, the eddy viscosity is expressed as a functional form,

$$\mu_t = (\mu_t)_o[1 - \exp(-(\mu_t)_i/(\mu_t)_o)]. \tag{23}$$

Here τ_m is the maximum Reynolds shear stress, n is the local normal distance from the wall, κ is the von Karman constant ($=0.418$), and D is the damping factor given by

$$D = 1 - \exp(-\rho_w n \max(u_m, u_w)/\mu_w A^+), \quad u_m = \sqrt{\tau_m}, \quad u_w = \sqrt{\tau_w/\rho_w}, \tag{24}$$

where $A^+ = 17$ and τ_w is the wall shear stress.

The Reynolds shear stress is evaluated by

$$\tau = \mu_t|\vec{\omega}|/\rho. \tag{26}$$

The maximum Reynolds shear stress, τ_m, is obtained by solving an ODE given in Reference [2]. In the three-dimensional case, this equation is given as [12]

$$\frac{\partial g}{\partial t} + U_m \frac{\partial g}{\partial x} + V_m \frac{\partial g}{\partial y} + W_m \frac{\partial g}{\partial z} + \Gamma = 0, \tag{27}$$

here reference quantities g and g_{eq} are introduced as $g = \tau_m^{-1/2}$ and $g_{eq} = (\tau_{m,eq})^{-1/2}$. The source term Γ is defined as

$$\Gamma = \frac{a_1}{2L_m}\left[\left(\frac{g}{g_{eq}} - 1\right) - \frac{C_D L_m |1 - \sigma^{1/2}|}{a_1 \delta (0.7 - n_{max}/\delta)}\right]. \tag{28}$$

The dissipation length scale L_m is expressed as

$$L_m = \min(0.4 n_m, 0.09\delta). \tag{29}$$

The coefficient σ in Equation (21) is introduced in the evaluation of $(\mu_t)_o$ to expose a match on two values of the maximum shear stress, one based on Equation (26) and the other obtained from the solution of the differential equation (27). At a new time level, the σ is updated using the following:

$$\sigma^{(n+1)} = \sigma^{(n)} \frac{\tau_m}{(\mu_t|\omega|/\rho)^{\max}}. \tag{30}$$

3.2.2. Some notes on the J–K model. The J–K model presented above is not the original one developed by Johnson and King [2]. Here it has been extended by Abid [12] and Radespiel [9] to three-dimensional computations. Further modifications have been made by other researchers. Marx [8] highlighted a problem arising in the evaluation of the maximum $\mu|\omega|/\rho$ and has given a detailed discussion on the behavior and function of $\mu|\omega|/\rho$. This is quite similar to the problem with $F(n)$, which has been reviewed in Section 3.1.2. However, no general way could be found to solve this problem. Johnson and Coakley [13] proposed some modifications to the original model to improve the predictions of skin friction. They suggested that the eddy viscosity evaluation can be done using

$$\mu_t = (\mu_t)_o \tanh[(\mu_t)_i/(\mu_t)_o],$$

and $\sqrt{(\rho_m/\rho_w)}u_m$ should be used instead of u_m. As for the inner layer viscosity, it's formula was modified as

$$(\mu_t)_i = (1.0 - \gamma_2)[(\mu_t)_i]_{M-L} + \gamma^2[(\mu_t)_i]_{J-K},$$

where the subscript M–L means using the mixing length model and J–K means using the Johnson–King model. The newly introduced quantity γ_2 was formulated as

$$\gamma_2 = \tanh\left(\frac{n}{L_c}\right),$$

$$L_c = \frac{\sqrt{\rho_w}u_\tau L_m}{\sqrt{\rho_w}u_\tau + \sqrt{\rho_m}u_m}.$$

Another suggestion was proposed as to the source term in the ODE. In the attached flow region, the second term in Equation (28) should be set to zero.

In this paper, all the above mentioned modifications to the J–K model have been adopted. The computed results show that predictions of pressure distribution on walls and the skin friction have been much improved.

3.3. Special treatment of multiwall situations

When a B–L or a J–K model is used for modeling internal flows, a problem might arise due to the existence of multiwalls. In the B–L model, there are two quantities related to the wall surfaces: n and $F(n)$, while the J–K model requires an integration of the ODE on a corresponding wall.

The simplest way is to use the shortest distance among those from different walls involved in the flow, and the final viscosity is also calculated referring to the corresponding wall. For some cases, e.g. 2D channel flow, the error may have no significant effect on the results. However, for backward-facing step flow or rectangular duct flow, where more than two walls exist, other methods [10,14] have to be applied for providing a more accurate approximation. In the J–K model, the shortest distance is first determined and the corresponding wall is chosen for the integration of the ODE over all the boundary cells. All the relevant quantities in the ODE are projected onto this corresponding wall surface. Then the solution can be obtained by the five stage Runge–Kutta time stepping scheme.

3.4. Point-implicit treatment to source terms

The ODE in the J–K model can be rewritten in the following integral form:

$$\frac{\mathrm{d}}{\mathrm{d}t}\int_{\Omega} g\,\mathrm{d}V + \int_{\partial\Omega} \vec{V}_{\mathrm{m}}\cdot\vec{n}\,\mathrm{d}S = \int_{\Omega} -\Gamma\,\mathrm{d}V, \tag{31}$$

where $\vec{V}_{\mathrm{m}} = \{U_{\mathrm{m}}, V_{\mathrm{m}}, W_{\mathrm{m}}\}$. The subscript m means that the velocity components are those in the cell where the Reynolds stress reaches its maximum value. The integration of Equation (31) is carried out over the surface cells on a solid wall. Therefore, the discretized form of Equation (31) can be written as

$$\frac{\Delta g}{\Delta t} = -\frac{Q_g}{\Delta V} + S_{\Gamma}, \tag{32}$$

where ΔV is the volume of a cell on the wall surface and S_{Γ} is the source term in the ODE, $S_{\Gamma} = -\Gamma$. The flux Q_g is defined as

$$Q_g = \sum_{f=1}^{4} (\vec{V}_{\mathrm{m}}\cdot\vec{n}\Delta S)_f;$$

here no flux calculation is needed at the two cell faces that are parallel to the wall surface.

It has been found that the explicit solutions of turbulence transport equations might encounter instability problems caused by source terms in these governing equations. The explicit numerical method for the ODE in the J–K model is found to be inadequate in obtaining a converged solution. Therefore, a point-implicit treatment is introduced for the source term in the ODE. This can be expressed as

$$\frac{\Delta g}{\Delta t} = -\frac{Q_g^n}{\Delta V} + S_{\Gamma}^{n+1}. \tag{33}$$

Here, the source term S_{Γ} is treated implicitly. By using the Taylor expansion, S_{Γ} at the $n+1$ time step can be evaluated as

$$S_{\Gamma}^{n+1} = S_{\Gamma}^{n} + \frac{\partial S_{\Gamma}}{\partial g}(g^{n+1} - g^{n}).$$

Then, Equation (33) becomes

$$\frac{\Delta g}{\Delta t} = \frac{R_g^n}{1 - \Delta t\,\partial S_{\Gamma}/\partial g}, \tag{34}$$

where $R_g^n = Q_g^n/\Delta V + S_{\Gamma}^n$ and $\partial S_{\Gamma}/\partial g$ is easily obtained by

$$\frac{\partial S_{\Gamma}}{\partial g} = \frac{a_1}{2L_{\mathrm{m}}}. \tag{35}$$

In the time stepping procedure, the integration of $\Delta g/\Delta t$ can be divided to five stages, similar to that in the solution of Equation (5) for the mean flow. The numerical result shows that the present treatment is very effective in obtaining the converged solution.

4. NUMERICAL RESULTS AND DISCUSSION

4.1. Code validation

A two-dimensional flat plate turbulent boundary layer flow is first used to validate the code which incorporates the modified B–L and J–K models and the numerical strategies for the J–K model. The inflow Mach number is 0.3. The grids are $48 \times 40 \times 4$ and only stretched along the normal direction to the plate wall. A two level multigrid is used to obtain a faster convergence. The reduction of the residual order is above 4. Figure 1 and Figure 2 show the computed velocity profiles compared with the experimental log law curve, using both the B–L and the J–K models with their modifications.

4.2. Arc-bump channel flow case

A two-dimensional turbulent bump flow case has been investigated by Liu [5] and Liu and Squire [4], both by experimental measurements and by numerical simulations. However, the numerical methods adopted in their study did not have the capability to predict the flow separation. To improve the performance of numerical simulation, and also to verify the validation of present turbulence models and the special treatment to them, this flow case is again studied here by the present method with different turbulence models. A $148 \times 60 \times 2$ grid (shown in Figure 3) is used for the discretization of the flow domain which has an arc-bump with its chord length, 80.0 mm, whole length from inlet-to-outlet, 240.0 mm, and height, 62.5 mm. The Reynolds number based on the chord length is 1.6×10^6. The cell size of the near-wall region is set to allow at least three points within the sublayer. In Liu's study [5], several cases with different inlet Mach numbers were reported. Here, only a transonic flow case

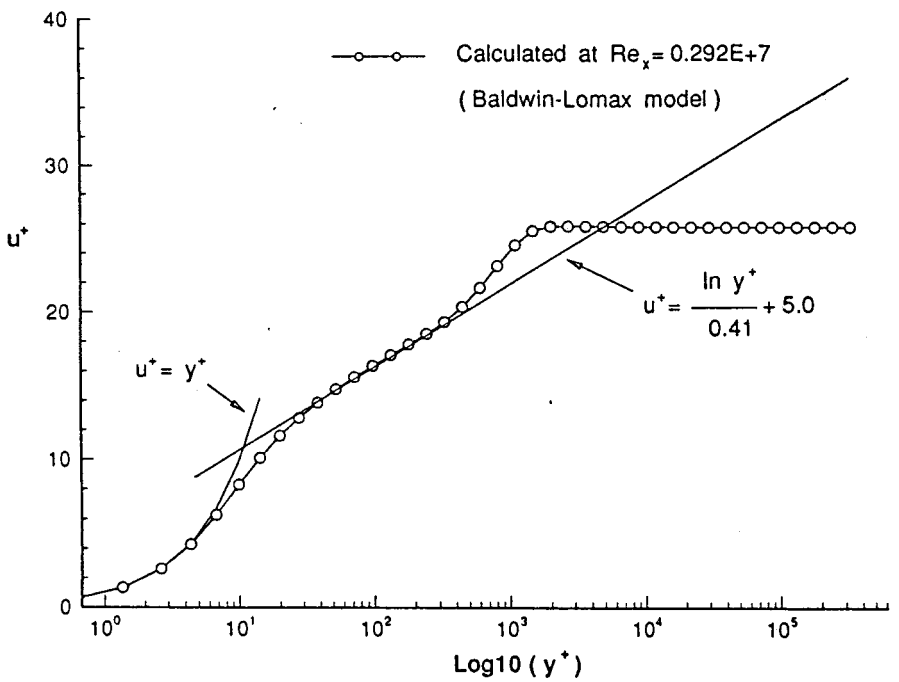

Figure 1. Log law profile by using the B–L model.

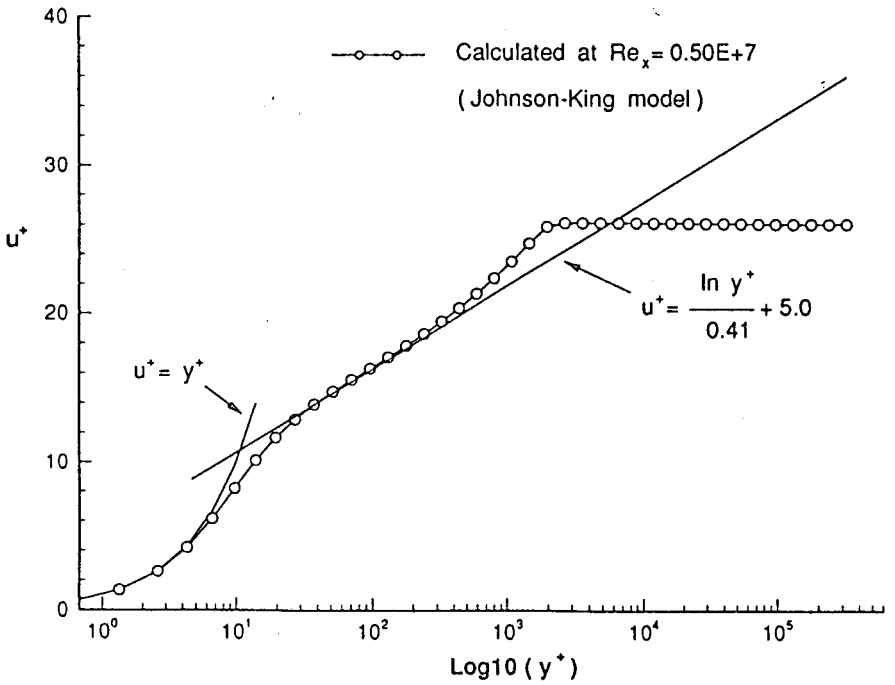

Figure 2. Log law profile by using the J–K model.

with a peak Mach number of 1.27 over the bump ($R = 163$ mm, the radius of the circular arc) is studied. In the present computation, the inlet Mach number is set to 0.675 and the back pressure is then adjusted to obtain a peak Mach number of 1.27 for comparison sake.

Boundary conditions for this channel flow were carefully handled with the available experimental data. At the upstream edge of the bump, the inflow Mach number and temperature are given as a free-stream condition. By the introduction of Riemann invariants for one-dimensional inviscid flow normal to the boundary, the non-reflecting boundary conditions are imposed. Flow quantities at this boundary are obtained in accordance with the condition that the Riemann variables for incoming and outgoing waves are constant along the normal direction. For the outflow boundary, all the flow quantities are linearly extrapolated from the flow domain, while the pressure is prescribed according to experimental measurement. At the solid walls, no-slip and no-injection boundary conditions are imposed, i.e. the zero normal fluxes of mass, momentum and energy are imposed. In addition, the solid surfaces are assumed to be adiabatic and the pressure gradient normal to the wall at the surface is considered to be zero.

All the computations are carried out on a NEC-SX3 supercomputer. Several different grids have been tested in the computation. The grid used here has been proved to be sufficiently refined. The iteration number used is 6000 for each calculation using the B–L or J–K model. The order of residual reduction for both computations is more than 4. The CFL number is chosen as 1.5 and both second-order and fourth-order artificial viscosities are used for reaching a stable shock-capturing calculation. For the B–L model case, the CPU time usage is 0.72 s per iteration, while it is 1.12 s per interaction for the J–K model.

Figure 4 presents a comparison between experimental interferogram and computed results using the B–L and J–K models. The zebra contour lines represent isodensity plotting. A

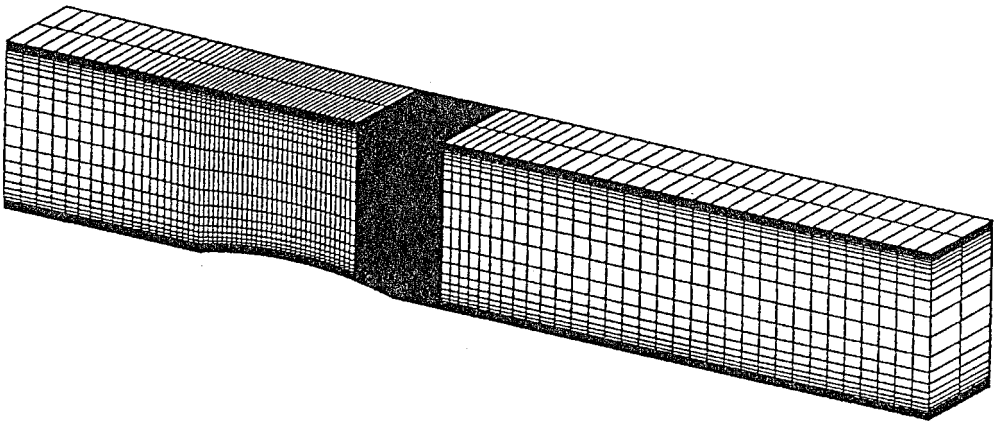

Figure 3. Grids for arc-bump channel flow.

curved shock is predicted by both models and agrees with the actual shock pattern. However, the prediction of the J–K model gives better agreement than that of the B–L model.

In Figure 5, by using both models, the predicted pressure distributions along the bump wall and the top wall are given and compared with the experimental data. Generally, the J–K model can better predict the pressure on both walls than the B–L one. A 'plateau' corresponding to the shock-induced separation region on the lower wall is well predicted. The velocity field details near the separation region are shown in Figure 6 using the B–L model and Figure 7 using the J–K model, where a recirculation zone is clearly present.

The skin friction coefficient on the bump wall can be obtained by using both models and the results are presented in Figure 8. A comparison is also presented in this figure between

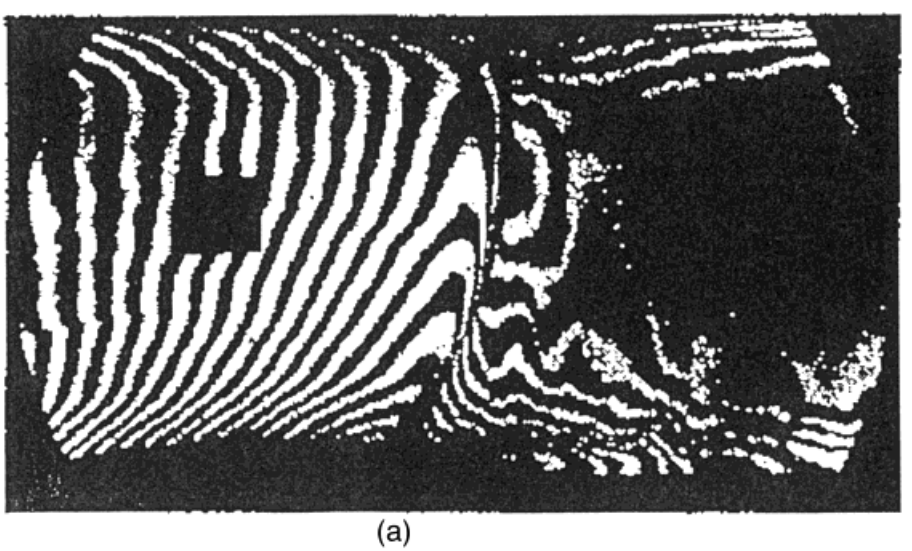

Figure 4. Comparisons of density contours by experiment, the B–L model and the J–K model.

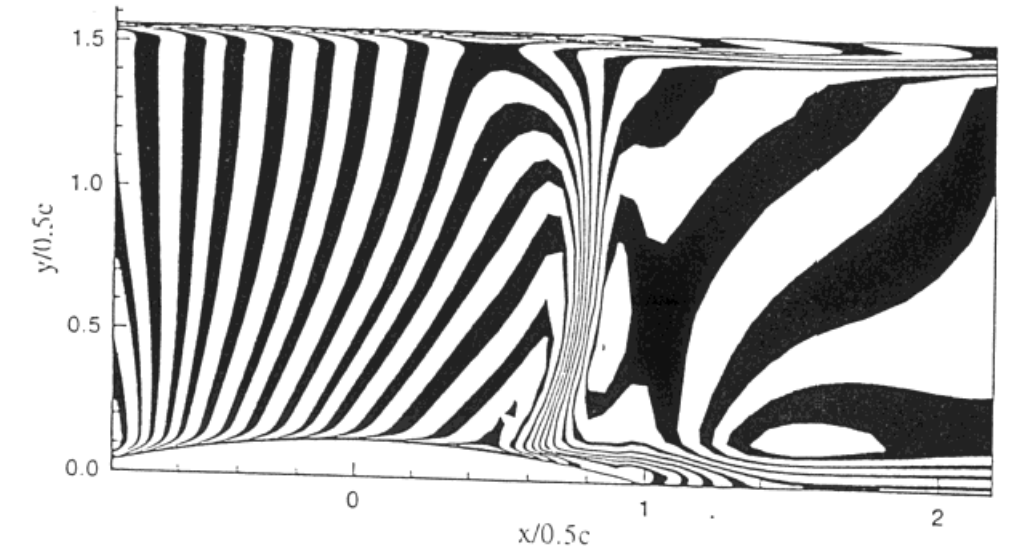

(b)

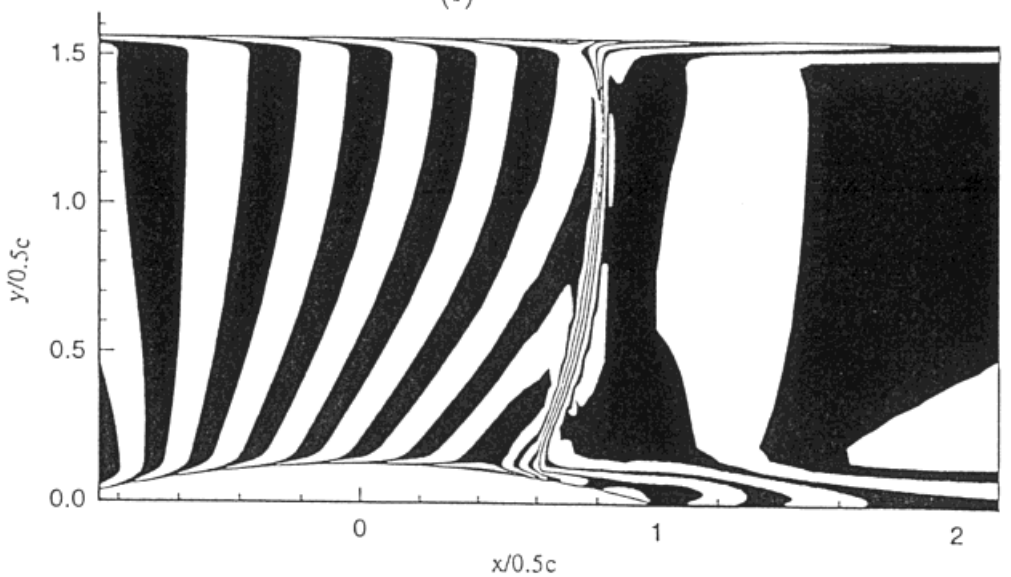

(c)

Figure 4 (*Continued*)

experimental data and the computed results by using other methods in Liu's study. It is observed that a separation region is clearly predicted with a very satisfactory accuracy with both the B–L and J–K models, with the latter predicting the size of the separation zone more accurately. All the methods in Liu's paper failed to do so. After the reattachment, however, the predicted skin friction coefficient by the J–K model is higher than both the B–L model's results and the experimental data. It seems that in the attached flow region, the B–L model can probably give a better skin friction coefficient than the J–K model.

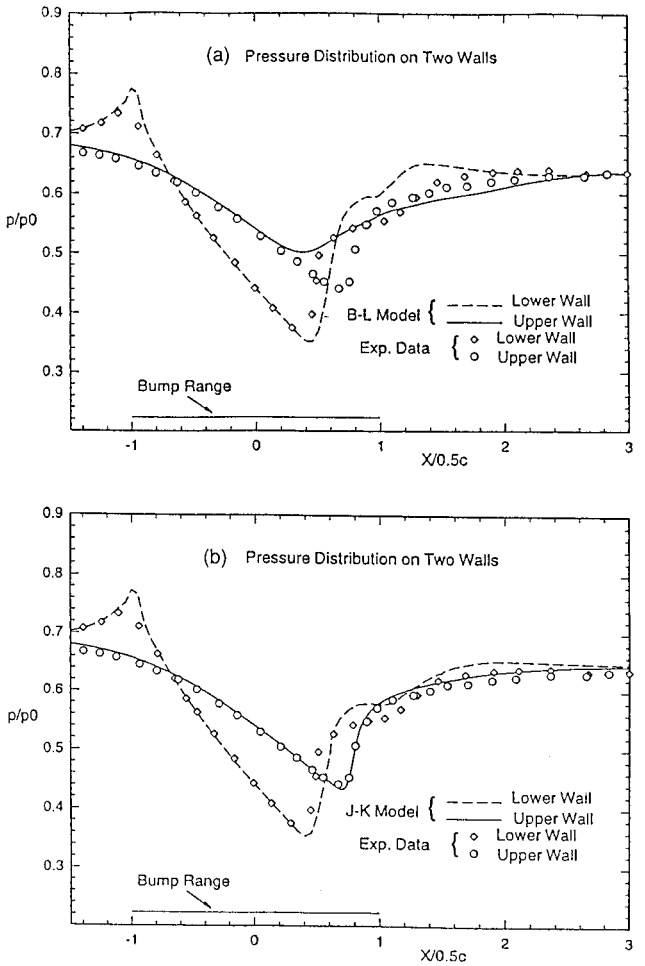

Figure 5. Pressure distribution on walls by using (a) the B–L model and (b) the J–K model.

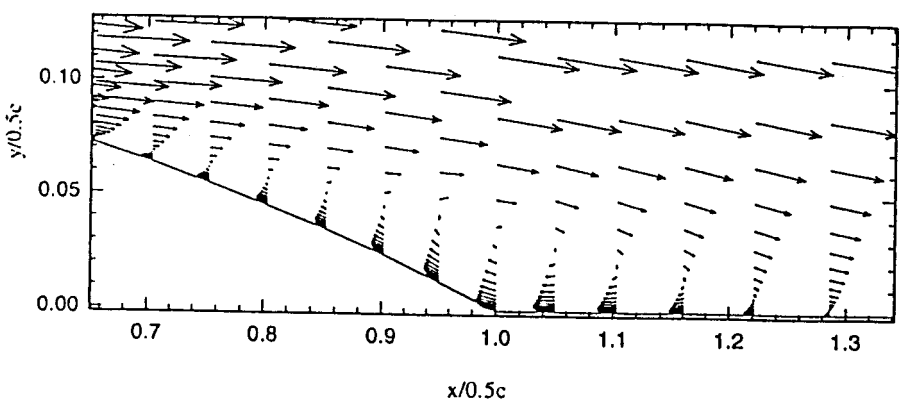

Figure 6. Velocity field in separation region by using the B–L model.

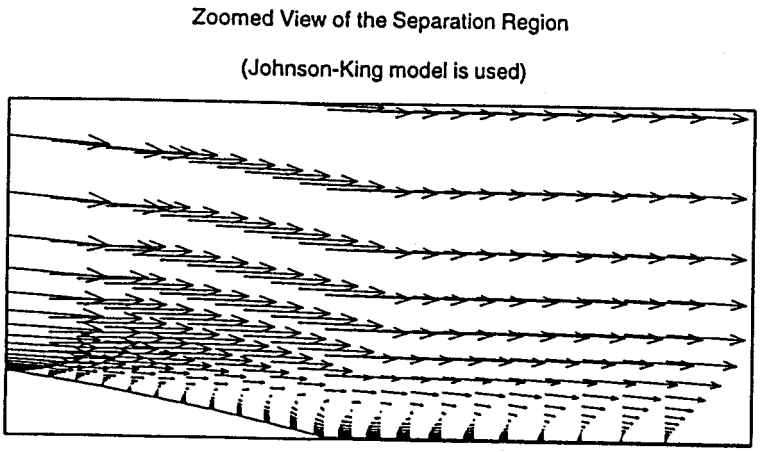

Figure 7. Velocity field in separation region by using J–K model.

The velocity profiles at different locations have been obtained by Liu and Squire's experiment and are used here for validating the present computation. In Figure 9, the computed velocity profiles are compared with measurements. The predictions by the present modified B–L and J–K models agree with the experimental data very well.

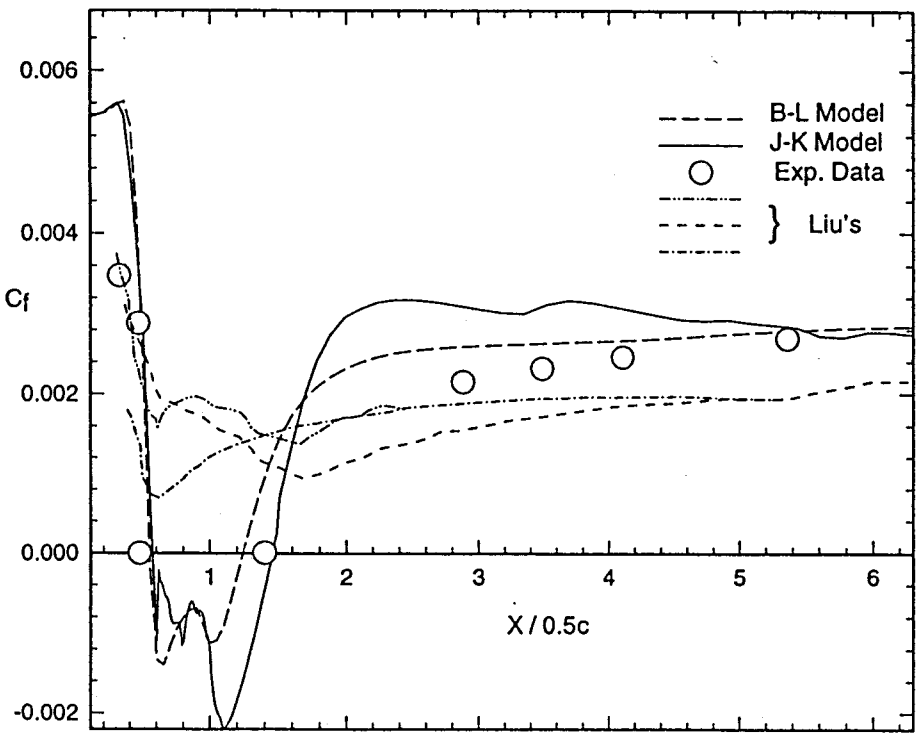

Figure 8. Skin friction coefficients on the lower bump wall.

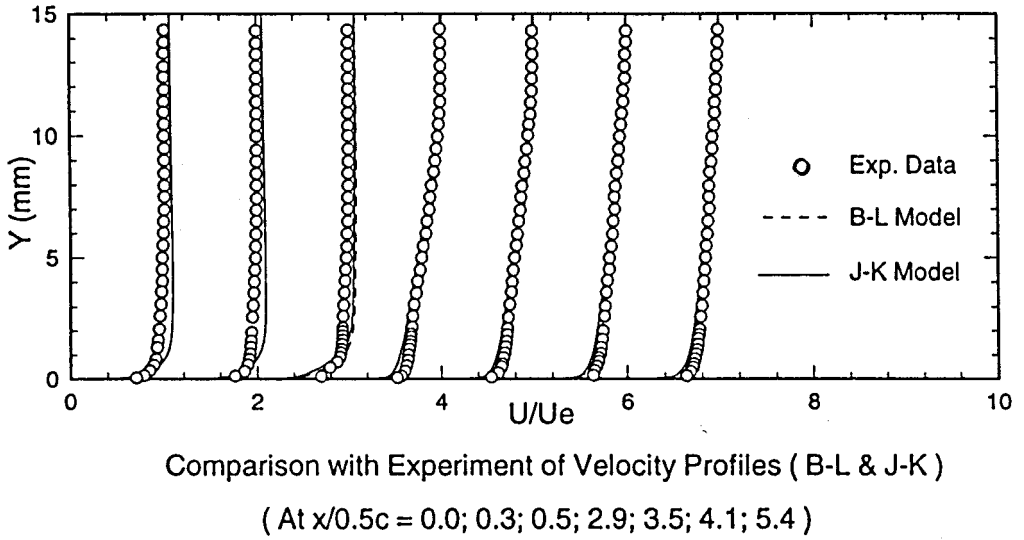

Figure 9. Comparison with experiment of velocity profiles.

5. CONCLUSION

(1) Two turbulence models, the B–L model and the J–K model, hvae been used in the present study. In order to improve the predictive capability of both models to deal with a complicated flow case, where shock–boundary interactions and subsequent separation occur, some modifications have been adopted.

(2) Especially for internal flow, a multiwall situation has been considered in the implementation of both models. The ODE in the J–K model is treated in a special way in that the equations along each wall around the flow field are solved respectively by projecting all the relevant quantities on to the wall surface. This proves to be successful.

(3) An explicit algorithm is used to obtain the solution of the ODE in the J–K model. Difficulties were encountered in obtaining stable and convergent solutions by this method. Therefore, a point-implicit treatment to the source term is introduced in the numerical solution of the J–K equation. This was shown to be a critical measure in ensuring a converged solution.

(4) A Q3D arc-bump channel flow with shock–boundary layer interactions and induced flow separation was studied. Both models can give satisfactory predictions for the major flow characteristics and also details of the mean flow field. After applying modifications and special treatments, the J–K model is found to give better predictions for the computation of separated flows.

6. NOMENCLATURE

c	chord length of the circular-arc model
c_f	skin friction coefficient
D_i	artificial dissipation along the ξ-direction
e	internal energy per unit mass

E	total internal energy per unit mass
f	index of cell faces
$\vec{F}$	flux vector
g	$g = \tau_m^{-1/2}$
H	enthalpy
J	Jacobian matrix
l	mixing length for turbulent viscosity
L_m	dissipation length scale
M	flow Mach number
n	local normal distance from the wall
n^+	law of the wall co-ordinate
$\vec{n}$	normal unit vector
p	pressure
Q_c, Q_v	convective flux and viscous flux
t	time
T	temperature
u, v, w	mean velocity components in the x-, y- and z-directions
u_τ	wall shear velocity
$\vec{U}$	mean velocity vector (u, v, w)
(U_m, V_m, W_m)	velocity vector projected on the surface where Reynolds stress is maximum
ΔV	control volume

Greek letters

γ	specific heat ratio
$\bar{\lambda}$	scaling factor (based on the spectual radii of flux Jacobian matrix)
δ	thickness of boundary layer
ρ	density
μ	dynamic viscosity
μ_l	molecular viscosity
μ_t	turbulent viscosity
$(\mu_t)_i$, $(\mu_t)_o$	inner layer turbulent viscosity, outer layer turbulent viscosity
ξ, η, ζ	local curvilinear co-ordinates
$\vec{\omega}$	vorticity vector
$\kappa^{(2)}$, $\epsilon^{(2)}$	coefficients for artificial dissipation of second difference type
$\kappa^{(4)}$, $\epsilon^{(4)}$	coefficients for artificial dissipation of fourth difference type
Ω	flow domain
$\delta\Omega$	boundary of the flow domain
$\bar{\bar{\tau}}$	stress tensor
τ_m	maximum Reynolds shear stress across boundary layer
τ_w	wall shear stress

Superscripts

m	stage index of multistage scheme
n	time step counter

Subscripts

eq	evaluated by equilibrium model
l	laminar quantity
m	maximum value across the boundary layer
t	turbulent quantity
w	value on a wall

ACKNOWLEDGMENTS

The authors are grateful to the Center of Graphics and Imaging Technology (CGIT) at Nanyang Technological University (Singapore) and to the National Supercomputer Research Center (NSRC, Singapore) for providing the computing resources.

REFERENCES

1. B.S. Baldwin and H. Lomax, 'Thin layer approximation and algebraic model for separated turbulent flows', *AIAA paper 78-257*, 1978.
2. D.A. Johnson and L.S. King, 'A mathematically simple turbulence closure model for attached and separated turbulent boundary layers', *AIAA J.*, **23**, 1684–1692 (1985).
3. J.M. Delery, 'Experimental investigation of turbulence properties in transonic shock–boundary layer interactions', *AIAA J.*, **21** (1983).
4. X. Liu and L.C. Squire, 'Interaction on curved surface at transonic speed', in J. Delery (ed), *Turbulent Shear Layer–Shock Wave Interactions*, Springer, Berlin, 1986, pp. 93–104.
5. X. Liu, 'Shock–boundary layer interaction on curved surfaces at transonic speeds', *Ph.D. Dissertation*, Engineering Department, University of Cambridge, 1985.
6. A. Jameson, W. Schmidt and E. Turkel, 'Numerical solutions of the Euler equations by finite volume methods using Runge–Kutta time stepping schemes', *AIAA paper 81-1259*, 1981.
7. D. Degani and L.B. Schiff, 'Computation of turbulent supersonic flows around pointed bodies having crossflow separation', *J. Comput. Phys.*, **66**, 173–196 (1986).
8. Y.P. Marx, 'A practical implementation of turbulence models for the computation of three-dimensional separated flows', *Int. J. Numer. Methods Fluids*, **13**, 775–796 (1991).
9. R. Radespiel, 'A cell–vertex multigrid method for the Navier–Stokes equations', *NASA Tech. Memo. 101557*, NASA, 1989.
10. U.C. Goldberg and S.R. Chakravarthy, 'Prediction of separated flows with a new backflow turbulence model', *AIAA J.*, **26**, 405–408 (1988).
11. D.A. Johnson, 'Transonic separated flow prediction with an eddy viscosity–Reynolds stress closure model', *AIAA J.*, **25**, 252–259 (1987).
12. R. Abid, V. Vasta, D.A. Johnson and B.W. Wedan, 'Prediction of separated transonic wing flows with non-equilibrium algebraic turbulence model', *AIAA J.*, **28**, 1426–1431 (1990).
13. D.A. Johnson and T.J. Coakley, 'Improvements to a non-equilibrium algebraic turbulence model', *AIAA J.*, **28**, 2000–2003 (1990).
14. R.V. Chima and J.W. Yokota, 'Numerical analysis of three-dimensional viscous internal flows', *AIAA J.*, **28**, 798–806 (1990).

